Supporting Information

Synthesis, Detailed Characterization and Theoretical Understanding of Mononuclear Chromium(III)-Containing Polyoxotungstates $[Cr^{III}(HX^{V}W_7O_{28})_2]^{13-}$ (X = P, As) with Exceptionally Large Magnetic Anistropy

Wenjing Liu,[†] Jonathan H. Christian,[‡,§] Rami Al-Oweini,[†] Bassem S. Bassil,[†] Johan van Tol,[§] Mihail Atanasov,[*,ǁ,⊥] Frank Neese,[*,⊥] Naresh S. Dalal,[*,‡,§] and Ulrich Kortz[*,†]

[†]Jacobs University, School of Engineering and Science, P.O. Box 750561, 28725 Bremen, Germany

[‡]Department of Chemistry and Biochemistry, Florida State University, 95 Chieftan Way, Tallahassee, Florida 32306, United States

[§]National High Magnetic Field Laboratory, Florida State University, 1800 E Paul Dirac Drive, Tallahassee, Florida 32306, United States

[ǁ]Max-Planck Institute for Chemical Energy Conversion, Stiftstr. 34-36, 45470 Mülheim/Ruhr, Germany

[⊥]Institute for General and Inorganic Chemistry, Bulgarian Academy of Sciences, 1113 Sofia, Bulgaria

Corresponding Authors

*Prof. U. Kortz, Fax (+49) 421-200-3229
E-mail u.kortz@jacobs-university.de
Homepage www.jacobs-university.de/ses/ukortz

* Prof. N. Dalal, dalal@chem.fsu.edu

* Prof. F. Neese, Frank.Neese@cec.mpg.de

* Prof. M. Atanasov, mihail.atanasov@cec.mpg.de

Table S1. Survey of reported polyanions containing heptatungstate and heptamolybdate fragments.

Fragment	Structure type*	Formula	Ref.
{XW_7}			
{PW_7}	a	$[Ru(dmso)_3HPW_7O_{28}]^{6-}$ $[Fe^{III}(HPW_7O_{28})_2]^{13-}$ $[Co^{II}(HPW_7O_{28})_2]^{14-}$ $[Cd^{II}(HPW_7O_{28})_2]^{14-}$ $[Mn^{II}(HPW_7O_{28})_2]^{14-}$ $[Mn^{III}(HPW_7O_{28})_2]^{13-}$	1
{AsW_7}	a	$[Ru(dmso)_3HAsW_7O_{28}]^{6-}$	1a
{VW_7}	a	$[Ru(dmso)_3HVW_7O_{28}]^{6-}$	2
{TeW_7}	b	$[Te_2W_{16}O_{58}(OH)_2]^{14-}$ $[Te_2W_{18}O_{62}(OH)_2]^{10-}$	3
{CoW_7}	c	$[Co_7(H_2O)_2(OH)_2P_2W_{25}O_{94}]^{16-}$	4
{XMo_7}			
{$AsMo_7$}	c	$[Cr^{III}_2(As^{III}Mo_7O_{27})_2]^{12-}$ $[Cu^{II}_2(As^{III}Mo_7O_{27})_2]^{14-}$ $[Fe^{III}Cr^{III}(As^{III}Mo_7O_{27})_2]^{12-}$ $[Fe^{III}_2(As^{III}Mo_7O_{27})_2]^{12-}$	5
{$FeMo_7$}	c	$[As^{III}_2Fe^{III}_6Mo_{22}O_{85}(H_2O)]^{14-}$	6

* See Figure S2 for details.

Table S2. Selected bond lengths (Å) and angles (°) for polyanions **1a** and **2a**.

Polyanion 1a			
W(1)–O(1T)	1.716(5)	W(1)–O(156)	1.909(5)
W(2)–O(2T)	1.727(5)	W(1)–O(147)	1.899(5)
W(3)–O(3T)	1.731(5)	W(1)–O(12)	1.913(5)
W(4)–O(4T)	1.716(5)	W(1)–O(13)	1.943(5)
W(5)–O(5T)	1.743(5)	W(1)–O(2P)	2.340(5)
W(6)–O(6T)	1.734(5)	Cr–O(3A)	1.953(5)
W(7)–O(7T)	1.733(5)	Cr–O(2A)	1.956(5)
O(1T)–W(1)–O(147)	102.1(2)	Cr–O(4P)	1.996(5)
O(1T)–W(1)–O(156)	104.1(2)	O(3A)–Cr–O(2A)	90.12(19)
O(147)–W(1)–O(156)	91.4(2)	O(3A)–Cr–O(4P)	88.92(19)
O(147)–W(1)–O(12)	157.5(2)	O(2A)–Cr–O(4P)	91.47(19)
Polyanion 2a			
W(1)–O(1T)	1.713(5)	W(1)–O(170)	1.893(4)
W(2)–O(2T)	1.728(5)	W(1)–O(136)	1.908(5)
W(3)–O(3T)	1.746(5)	W(1)–O(12)	1.920(5)
W(10)–O(10T)	1.737(5)	W(1)–O(15)	1.953(5)
W(5)–O(5T)	1.733(5)	W(1)–O(1A1)	2.308(5)
W(6)–O(6T)	1.745(5)	Cr–O(5A)	1.953(5)
W(7)–O(7T)	1.721(5)	Cr–O(2A)	1.975(5)
O(1T)–W(1)–O(170)	102.5(2)	Cr–O(O3A1)	1.998(5)
O(1T)–W(1)–O(136)	104.6(2)	O(5A)–Cr(1)–O(2A)	90.2(2)
O(170)–W(1)–O(136)	90.6(2)	O(5A)–Cr(1)–O(3A1)	90.0(2)
O(136)–W(1)–O(12)	88.5(2)	O(2A)–Cr(1)–O(3A1)	92.7(2)

Table S3. Bond valence sum (BVS) values for different structural types of bridging oxygen atoms in $Na_{13}[Cr^{III}(HP^{V}W_7O_{28})_2]\cdot 47H_2O$ (**1**) and $Na_{13}[Cr^{III}(HAs^{V}W_7O_{28})_2]\cdot 52H_2O$ (**2**).

1		**2**	
μ_4-O (P, 3W)	**BVS value**	**μ_4-O (As, 3W)**	**BVS value**
O2P	2.052	O1A1	2.169
μ_3-O (3W)	**BVS value**	**μ_3-O (3W)**	**BVS value**
O147	1.873	O136	1.870
O156	1.892	O170	1.869
μ_2-O	**BVS value**	**μ_2-O**	**BVS value**
O23	1.890	O2A	1.811
O26	2.007	O5A	1.833
O56	1.951	O3A1	1.840
O45	1.844	O15	1.772
O47	1.879	O12	1.822
O37	2.036	O36	1.924
O12	1.834	O73	1.827
O13	1.799	O37	0.993
O46	0.993	O25	1.892
O1P	1.655	O15	1.726
O3P	1.763	O510	2.012
O4P	1.746	O26	1.979
O2A	1.823	O710	1.870
O3A	1.838	O2A1	1.690

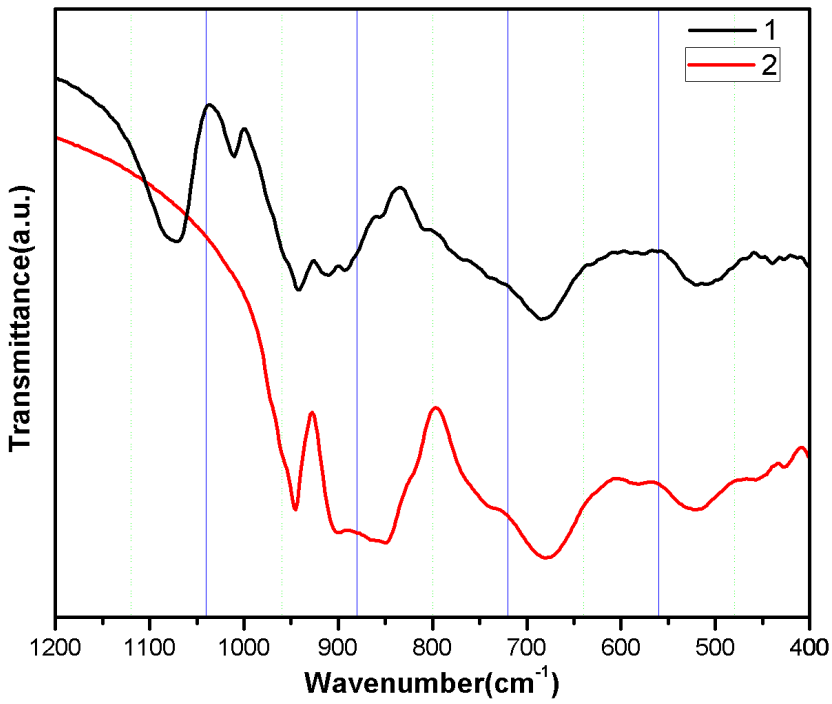

Figure S1. IR spectra of **1** and **2**.

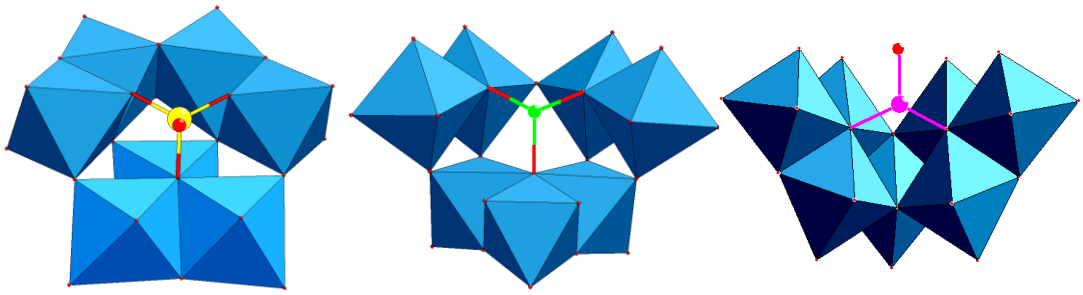

(**a**) (**b**) (**c**)

Figure S2. Polyhedral representation of the structural fragments $\{PW_7\}$ (a), $\{TeW_7\}$ (b), and $\{CoW_7\}$ (c). Color code: WO_6 octahedra (blue), P (yellow), Te (bright green), Co (pink), O (red).

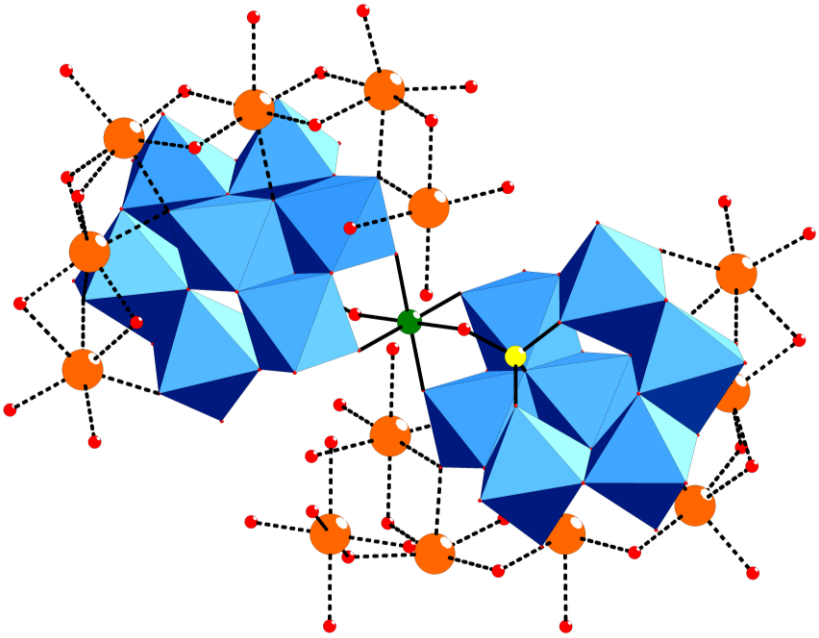

Figure S3. Representation of polyanion **1a** and its surrounding Na^+ counter cations (large orange balls). Water molecules are shown as small red balls, and the $Na^+\cdots OH_2$ interactions as dashed lines.

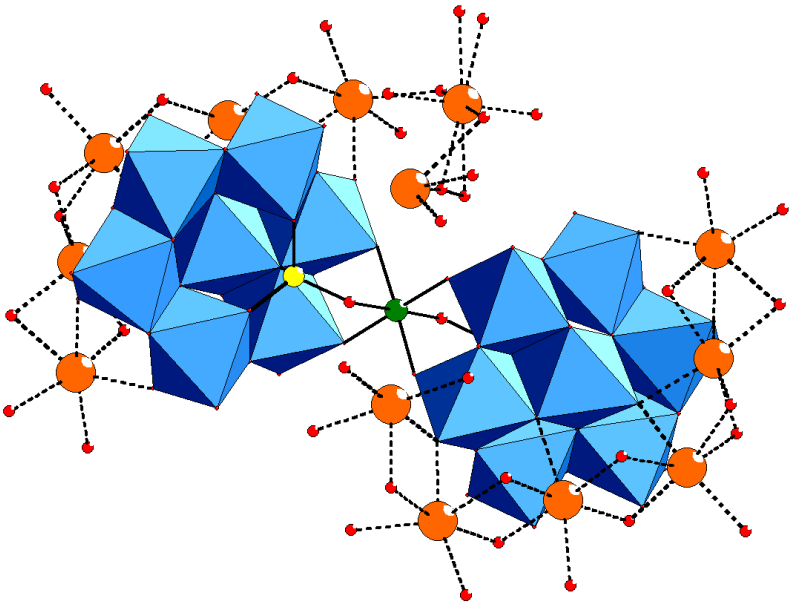

Figure S4. Representation of polyanion **2a** and its surrounding Na^+ counter cations (large orange balls). Water molecules are shown as small red balls, and the $Na^+\cdots OH_2$ interactions as dashed lines.

.

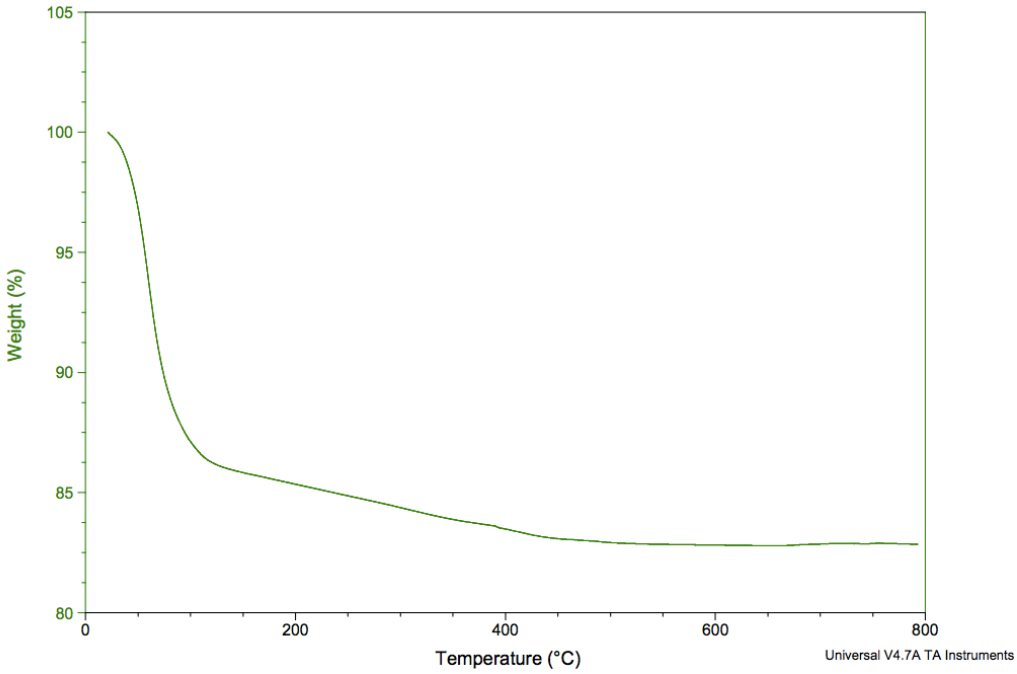

Figure S5. TGA curve for **1** ramped from room temperature to 800 °C.

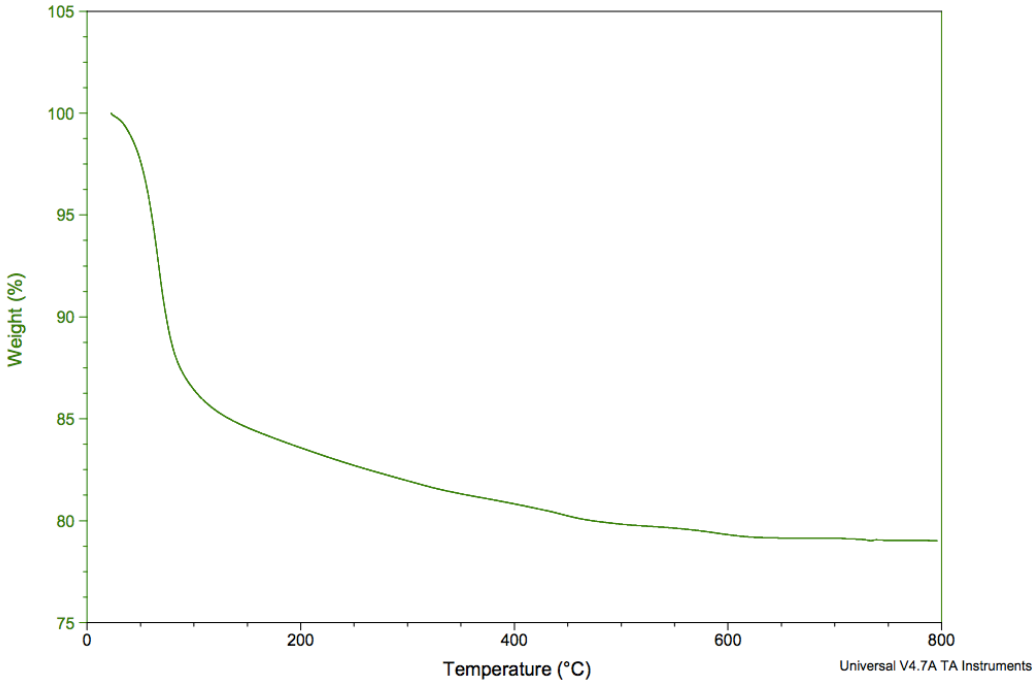

Figure S6. TGA curve for **2** ramped from room temperature to 800 °C.

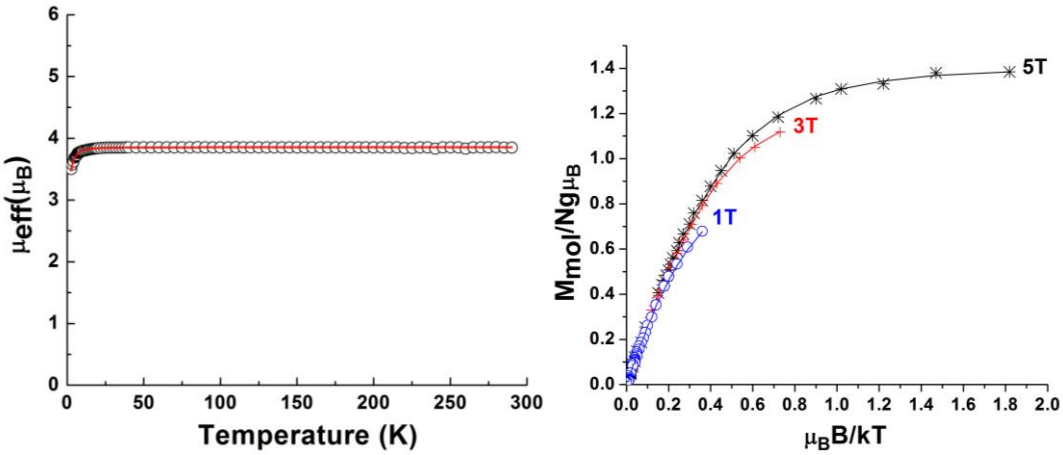

Figure S7. Left: μ_{eff} versus T of compound **1**. Right: VTVH magnetization measurements of **1** at 1, 3, and 5 T. The solid lines represent the best fits to the experimental data.[7]

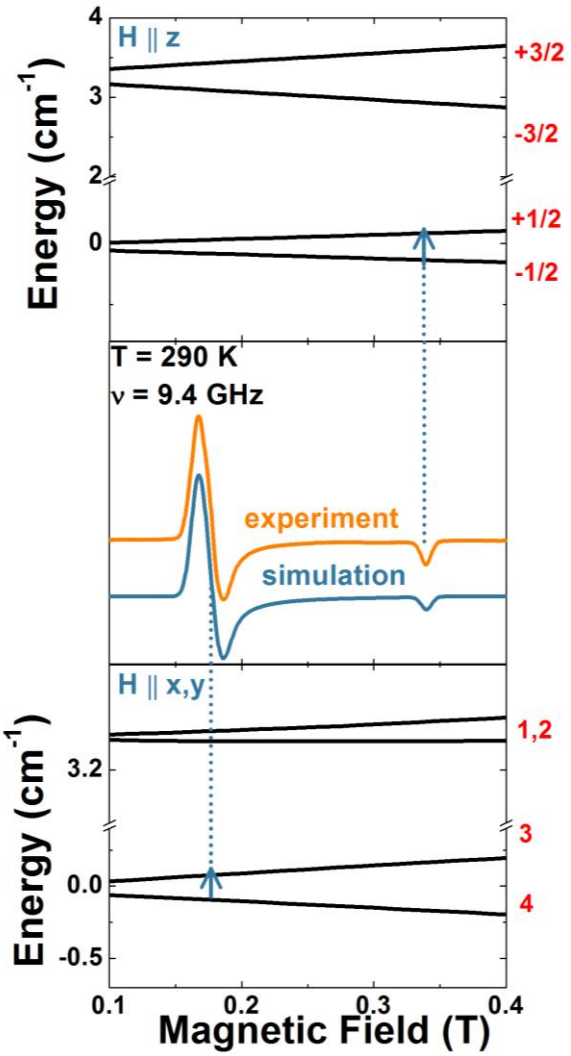

Figure S8. X-band (9.5 GHz) EPR experimental and simulation spectra of **1**. The top and bottom portions show the energy level diagrams for the H || z (principal symmetry axis of the molecule) and the perpendicular x, y directions. The red numbers in the top figure represent the M_s quantum numbers in the high-field limit. In the bottom figure, however, they are just a label for an energy level since the field strength was not sufficient to be in the 'high-field' limit. Blue arrows mark the EPR transition assignment.

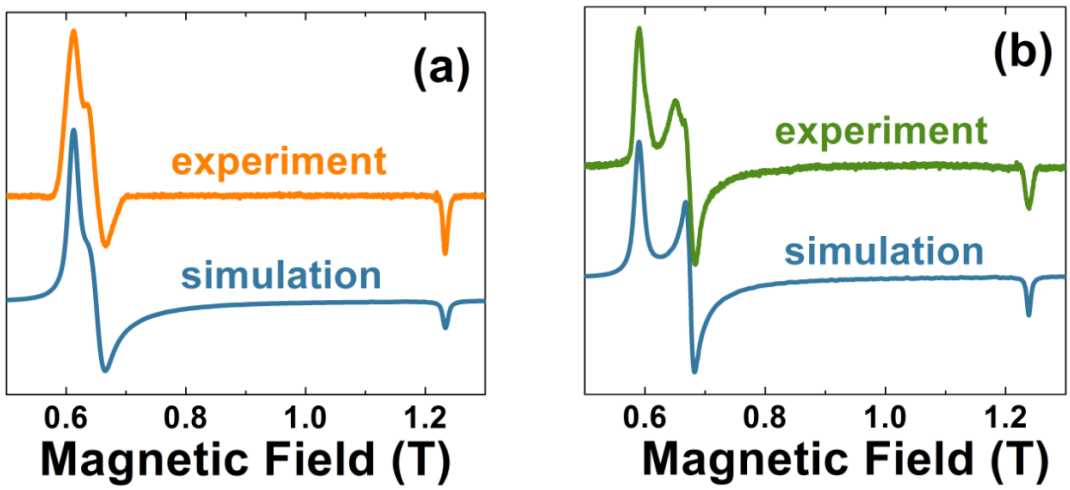

Figure S9. Q-band (34 GHz) EPR experimental and simulation spectra measured at room temperature for compounds **1** (a) and **2** (b).

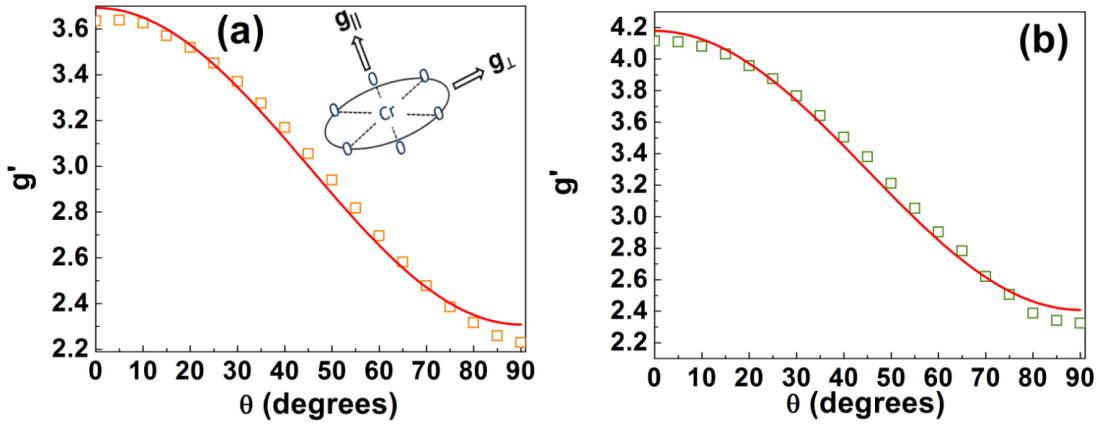

Figure S10. Single-crystal angular dependence Q-band (34 GHz) EPR spectra measured at room temperature. The results are fit to $g'^2=g_{\parallel}'^2\cos^2(\theta)+ g_{\perp}'^2\sin^2(\theta)$, which describes the angular dependence of the g factor for single crystals in an axially symmetric environment for compounds **1** (a) and **2** (b).[8]

References

(1) (a) Bi, L.-H.; Dickman, M. H.; Kortz, U.; Dix, I. *Chem. Commun.* **2005**, 3962−3964; (b) Wu, Q.; Li, Y.-G.; Wang, Y.-H.; Zhang, Z.-M.; Wang, E.-B. *Inorg. Chem. Commun.* **2010**, *13*, 66−69; (c) Zhang, D.; Zhang, Y.; Zhao, J.; Ma, P.; Wang, J.; Niu, J. *Eur. J. Inorg. Chem.* **2013**, *2013*, 1672−1680.

(2) Bi, L.-H.; Wang, B.; Hou, G.-F.; Li, B.; Wu, L.-X. *CrystEngComm.* **2010**, *12*, 3511−3514.

(3) Ritchie, C.; Alley, K. G.; Boskovic, C. *Dalton Trans.* **2010**, *39*, 8872−8874.

(4) Clemente-Juan, J. M.; Coronado, E.; Forment-Aliaga, A.; Galán-Mascarós, J. R.; Giménez-Saiz, C.; Gómez-García, C. J. *Inorg. Chem.* **2004**, *43*, 2689−2694.

(5) (a) Li, L.; Shen, Q.; Xue, G.; Xu, H.; Hu, H.; Feng, F.; Wang, J. *Dalton Trans.* **2008**, 5698−5700; (b) Xu, H.; Li, L.; Liu, B.; Xue, G.; Hu, H.; Fu, F.; Wang, J. *Inorg. Chem.* **2009**, *48*, 10275−10280.

(6) Liu, B.; Li, L.; Zhang, Y.; Ma, Y.; Hu, H.; Xue, G. *Inorg. Chem.* **2011**, *50*, 9172−9177.

(7) Weil, J. A.; Bolton, J. R., *Electron Paramagnetic Resonance Elementary Theory and Practical Applications, 2nd ed.* Wiley−Interscience: Hoboken, NJ, , 2007, p. 90.

(8) Simulation of the experimental magnetic data was performed with the *julX* program (E. Bill: Max-Planck Institute for Chemical Energy Conversion, Mülheim/Ruhr, Germany)